Bioorg. Med. Chem. Lett. 41 (2021) 128024

Contents lists available at ScienceDirect

Bioorganic & Medicinal Chemistry Letters

journal homepage: www.elsevier.com/locate/bmcl

Design and synthesis of zinc protoporphyrin IX-adamantane/cyclodextrin/cellulose nanocrystals complexes for anticancer photodynamic therapy

Gautier M.A. Ndong Ntoutoume, Robert Granet, Jean-Pierre Mbakidi, Eléna Constantin, Ludovic Bretin, David Y. Léger, Bertrand Liagre, Vincent Chaleix, Frédérique Brégier, Vincent Sol *

Université de Limoges, PEIRENE EA 7500, 87060 Limoges, France

ARTICLE INFO

Keywords:
Cellulose nanocrystals
Porphyrins
Photodynamic therapy
Colorectal cancer
Nanoparticles

ABSTRACT

Two protoporphyrin IX (PpIX) adamantane derivatives were synthesized and then metallated with zinc. The Zn-PpIX derivatives, exhibiting a high singlet oxygen quantum yield, were tested for their photodynamic activity against the HT-29 cell line. In order to enhance their water-solubility and their cellular bioavailability, these photosensitizers were encapsulated into the hydrophobic cavity of cyclodextrins (CD) previously attached to cellulose nanocrystals (CNCs) via electrostatic interactions. Under illumination, the encapsulated adamantanyl-porphyrins exerted an enhanced in vitro cytotoxicity, as compared with the corresponding free photosensitizers.

Colorectal cancer (CRC) is considered the second-most commonly occurring cancer in women and the third in men. In the recent years, a rapid rise in colorectal cancer incidence and mortality has been observed in several developing countries.[1] A global increase of 60% of this malignancy incidence is expected by 2030.[2] A large portion of colorectal cancer patients who are treated with conventional chemotherapy eventually develop local recurrence or metastases. The failure of a complete cure in colorectal cancer patients may be related to the lack of complete eradication of cancer stem cells when using conventional therapy. Photodynamic therapy (PDT), also known as photochemotherapy or photoradiation therapy is an alternative experimental modality for the treatment of cancer. It is based upon the interaction between a photosensitizer (PS) and photons of visible light in presence of dioxygen, that results in the production of reactive oxygen species (ROS) and the subsequent death of tumor cells.[3,4] An important attribute of PDT is that the toxicity is confined to regions where the three components overlap spatiotemporally.[5] Protoporphyrin IX (PpIX), a natural and commercially available PS has been chosen for this work because of its high potential for treating a wide variety of tumors.[6,7] However, PpIX, as well as many PS, is known to have a poor selectivity and to be sparingly soluble in water. Nanotechnologies proved to be instrumental in designing tumor-targeted and water-soluble anticancer agents based on gold,[8] iron oxide,[9] or organic polymer nanoparticles.[10,11] This article describes the building of a photosensitizer based on cellulose nanocrystals (CNCs), a biocompatible nanomaterial which has already been used for this purpose.[12–14] CNCs were prepared from cellulose microfibrils by sulfuric acid hydrolysis. This hydrolysis preferentially destroys the amorphous zones of cellulose microfibrils and leaves the crystalline regions as *O*-sulfated derivatives.[15,16] The negatively charged nanoparticles were then complexed with positively charged cyclodextrin derivatives obtained from the functionalization of β–cyclodextrin with a quaternary ammonium. Cyclodextrin–CNCs ionic complexes were eventually loaded with mono- or di–adamantane–zinc–PpIX, thanks to the affinity of the hydrophobic cavity of cyclodextrin for apolar molecules. To evaluate the efficacy of the resulting nanobiomaterials and to validate the concept of vectorization by cellulose nanocrystals, in vitro bioassays were carried out against a colorectal cancer line (HT-29). Preliminary results allowed us to evaluate the ability of nanoparticles to enhance the bioavailability of PS in the cancer cells and to check that the photocytotoxic effects observed were actually attributable to the photosensitizers molecules which had been delivered inside the cells.

The synthesis of the adamantanyl protoporphyrin IX derivatives is summarized in Scheme 1.Protoporphyin glycol ester has been synthesized following previously reported procedure.[17] Briefly, protoporphyrin IX and excess ethylene glycol were mixed in presence of sulfuric acid (H_2SO_4, 96%) as catalyst, and stirred at room temperature during 1.5 h. Then the organic fraction was washed with demineralized water to

* Corresponding author.
E-mail address: vincent.sol@unilim.fr (V. Sol).

https://doi.org/10.1016/j.bmcl.2021.128024
Received 31 January 2021; Received in revised form 28 March 2021; Accepted 4 April 2021
Available online 9 April 2021

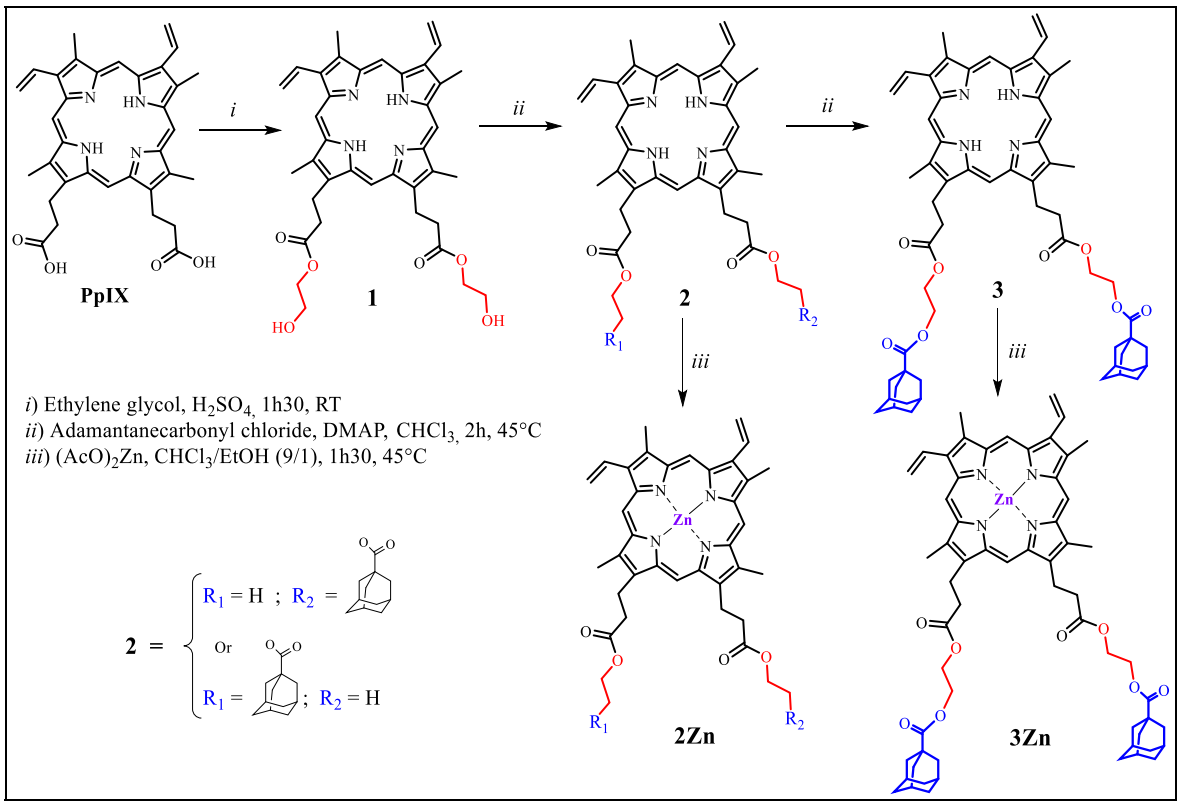

Scheme 1. Synthesis of adamantane–protoporphyrin IX derivatives.

remove unreacted ethylene glycol. The product was obtained in 80% yield after purification by preparative silica gel thin layer chromatography ($CHCl_3$/EtOH: 95/5). The reaction leads to the binding of two ethylene glycol units to protoporphyrin IX. The structure of compound **1** was confirmed by UV–Visible, MS and ^1H NMR (see SI and Table S1 and S2).

Attachment of one or two adamantane units to compound **1** was carried out through esterification of the ethylene glycol hydroxyls by adamantanecarbonyl chloride in chloroform and in presence of 4-dimethylaminopyridine (DMAP) as catalyst.[18] Compounds **2** and **3** were obtained in 60% and 70% yields, respectively. The structure of compounds **2** and **3** was confirmed by UV–Visible, MS and 1H NMR spectroscopy (see Supporting Information and Tables S1 and S2). The spectra of the synthesized protoporphyrinic derivatives (**1**, **2** and **3**) are of the "etio" type and are characteristic of the porphyrins substituted on the β-pyrrole positions. UV–visible spectra of compounds **2** and **3** display Soret bands at 408 nm and Q bands at 506, 542, 578 and 631 nm (Fig. S9). Zinc metalation of compounds **2** and **3** was carried out in a mixture of chloroform and ethanol ($CHCl_3$/EtOH: 8/2) in the presence of excess zinc acetate. The reaction was monitored by TLC for 2 h and then the solvent was evaporated to dryness and the crude product was purified by preparative column chromatography on silica ($CHCl_3$/EtOH: 95/5). **2Zn** and **3Zn** were obtained in excellent yields, 96% and 94%, respectively. Both molecules were characterized by UV–Visible, MS spectroscopy and ^1H NMR. UV–Visible spectra carried out in $CHCl_3$ (Fig. S9 and Tables S2) clearly showed the modification of the absorption spectrum with a slight redshift of the Soret band (from 408 nm to 415 to ~417 nm) and the disappearance of bands Q_I and Q_{II} (Table S2). Structures of all compounds were characterized by MS. The theoretical and experimental masses of the synthesized protoporphyrinic products are shown in Table S1.

Singlet oxygen is classically described as the toxic agent produced by tetrapyrrolic photosensitizers and dioxygen under illumination (type II mechanism). So, high $^1O_2$ quantum yields of photosensitizers are basic requirements for successful PDT. Singlet oxygen generating efficiencies of porphyrins were determined indirectly via the photooxidation of 9,10-dimethylanthracene (DMA) in DMF (Table 1).

The resulting zinc compounds **2Zn** and **3Zn** were then water-solubilized by encapsulation into cyclodextrins complexed to CNCs. The general route of this strategy, detailed in our previous study,[21] is presented in Scheme 2. It begins with the formation of cellulose nanocrystals and the functionalization of β–cyclodextrin with a quaternary ammonium in order to introduce the positive charges that will allow β-cyclodextrin to bind the CNCs via electrostatic interaction. Compounds **2Zn** and **3Zn** were then easily encapsulated into the cyclodextrin hydrophobic cavity (Fig. S2), with an approximate rate of 10% (i.e. mass of the different zinc porphyrinato derivatives, relative to the mass of **CD/CNCs** complexes). Indeed, size ranging from 100 to 400 nm, crystalline CNCs have physicochemical and mechanical properties such as high tensile strength and elastic modulus (130 ~ 150 GPa), a high specific surface (150 to 300 m^2/g), and a low density (1.6 g/cm^3).[22,23] These characteristics make these particles promising candidates for the selective delivery of biomolecules.[24] CNCs are obtained by hydrolysis of the amorphous domains of the cellulose by a strong acid, usually

Table 1
Singlet oxygen quantum yield of PPIX, Zn PPIX and Zn PPIX derivatives (**2Zn**, **3Zn**) in DMF.

Compounds	Singlet Oxygen quantum yield Φ_Δ $^1O_2$[a]
PpIX	0.81 ± 0.01
Zn PPIX	0.83 ± 0.01
2Zn	0.84 ± 0.02
3Zn	0.79 ± 0.02

[a] Mean of two independent experiments using tetraphenylporphyrin as standard (Φ_Δ = 0.64 in DMF) and 9,10-dimethylanthracene as decribed in supporting information.[19,20]

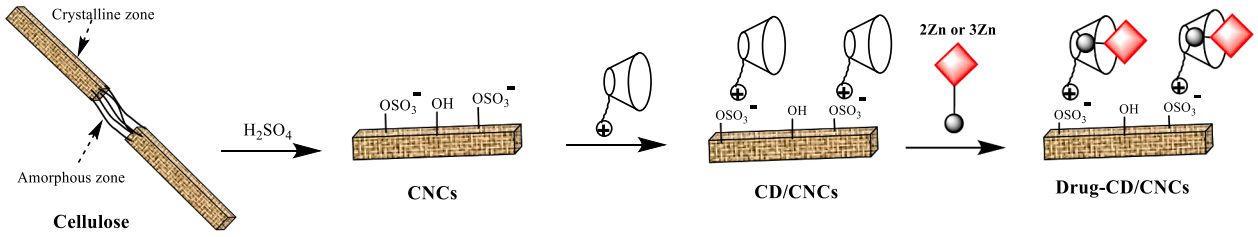

Scheme 2. General strategy of CNCs synthesis and encapsulation of **2Zn** and **3Zn** by **CD/CNCs**.

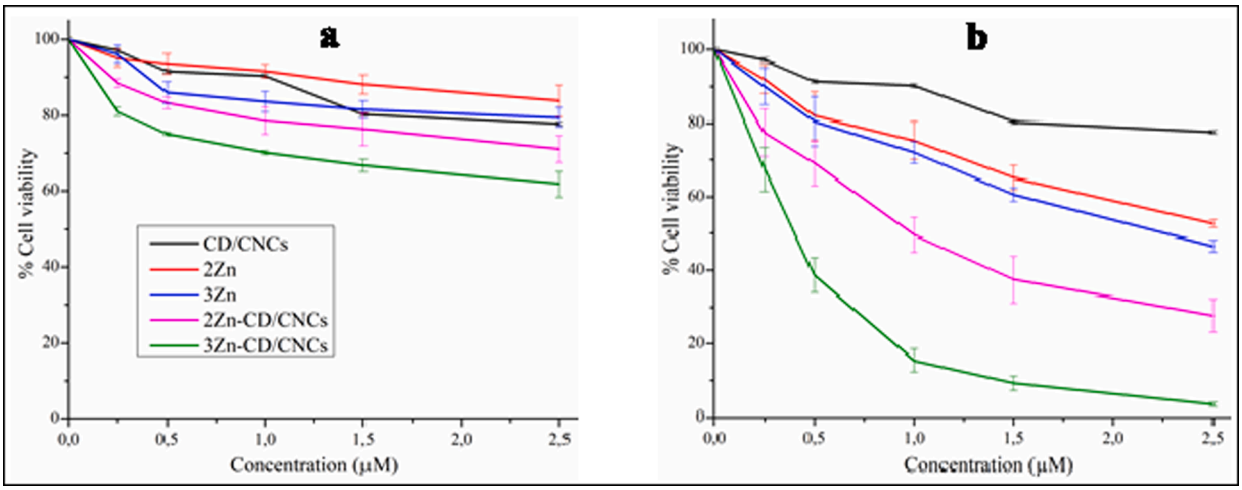

Fig. 1. Dose-dependent effects of **2Zn**, **3Zn** compounds (solubilized in DMSO), **CD/CNCs**, **2Zn–CD/CNCs** and **3Zn–CD/CNCs** complexes (in suspension in sterilized water) on the viability of HT-29 cells: a) in the dark, b) under illumination with white light (fluence rate 75 J.cm^{-2}). CD/CNCs (black curve) concentrations are the same that [CD/CNCs] with Zn-PpIX derivatives.

H_2SO_4.[25] Cellulose hydrolysis is accompanied with a sulfation process that creates negative charges (~209 to 250 mmol/kg) on the surface of these nano-objects.[26,27] These charges are responsible for the stability of the colloidal suspension of CNCs in aqueous solution.[15] Solvent-exposed hydroxyl groups of the nanoparticles not only make them hydrophilic but they also can participate to various chemical reactions.[28] For this work, size (DLS, dynamic light scattering), Polydispersity index (PDI) and zeta potential, XRD, TEM and other physicochemical characterizations of cellulose nanocrystals, cationic cyclodextrin and various platforms have been measured (see supporting information, Table S3 and Figs. S11–S15). A significant increase of the zeta potential of CNCs was observed, due to the positive charges brought by the cationic CDs (Table S3). After the inclusion complex formation between cyclodextrin and compounds **2Zn** and **3Zn**, the size of nanoparticles increase from 190.1 ± 5.1 nm to 210.1 ± 1.0 nm and 211.6 ± 1.2 nm respectively.

In vitro phototoxicity of **2Zn** and **3Zn** compounds, as well as **2Zn–CD/CNCs** and **3Zn–CD/CNCs** complexes was evaluated against the HT–29 colorectal cancer cell line, with the 3-(4,5-dimethylthiazol-2-yl) 2,5-diphenyl tetrazolium bromide (MTT) method. This evaluation was carried out in presence of photosensitizer concentrations ranging from 0.25 to 2.5 μM during 48 h in the dark and under illumination (Fig. 1). Within the concentration range tested, we observed a low cytotoxicity in the dark (Fig. 1a). Cell viability of HT-29 cells remained higher than 70%, in presence of free **2Zn** or **3Zn** compounds, and for **2Zn-CD/CNCs.** For **3Zn**-encapsulated into **CD/CNCs**, cell viability was around 60% at 2.5 μM (Fig. 1a). Under illumination, protoporphyrin cytotoxicity was much stronger in comparison with the control test in the dark (Fig. 1a and b).

Encapsulation of protoporphyrin derivatives into **CD/CNCs** significantly increased their toxicity, **3Zn–CD/CNCs** being the most active complex. IC_{50} values are reported in Table 2.

Only IC_{50} values of **3Zn** (2.5 ± 0.03), **2Zn-CD/CNCs** (1.0 ± 0.05) and **3Zn-CD/CNCs** (0.42 ± 0.02) were obtained. A flow cytometry analysis was conducted in support of the vectorization effect (Fig. 2A and B). For this purpose, HT-29 cancer cells were treated separately with free or vectorized Zn-PpIX derivatives at the same concentration (2.5 μM in drug) in DMSO (free PS) or in sterilized water for complexes. After 24 h incubation, fluorescence of the Zn-PpIX derivatives was analyzed by flow cytometry coupled with the AMNIS® image analysis. The first two graphs represent the size/structure ratio of HT-29 cells according to the treatments. Fluorescence intensities of individual cells were analyzed. The table summarizes the number of cells in the selected population as well as the number of Zn-PpIX positive cells according to the treatments. The intracellular fluorescence of zinc protoporphyrin is shown by representative images.

The AMNIS® flow cytometry results indicate that PS internalization is strongly improved when the cells are incubated with **2Zn** or **3Zn** complexed with CD/CNCs. Indeed, nearly all the treated cells exhibit

Table 2
IC_{50}* (μM) values from MTT assay with **2Zn**, **3Zn**, **CD/CNCs**, **2Zn –CD/CNCs** and **3Zn–CD/CNCs** against HT-29 cell lines in the dark and under illumination (white light, fluence rate 75 J.cm^{-2}).

Compounds	Illumination	Dark	IC_{50}dark/IC_{50}light
2Zn	>2.5	>2.5	ND**
3Zn	2.5 ± 0.03	>2.5	ND**
CD/CNCs	ND**	ND**	ND**
2Zn-CD/CNCs	1 ± 0.05	>2.5	>2.5
3Zn- CD/CNCs	0.42 ± 0.02	>2.5	>5.95

* IC_{50} values are the average of at least three determinations.
** Not determined when 70% or higher cell viability was recorded in presence of 2.5 μM of PS.

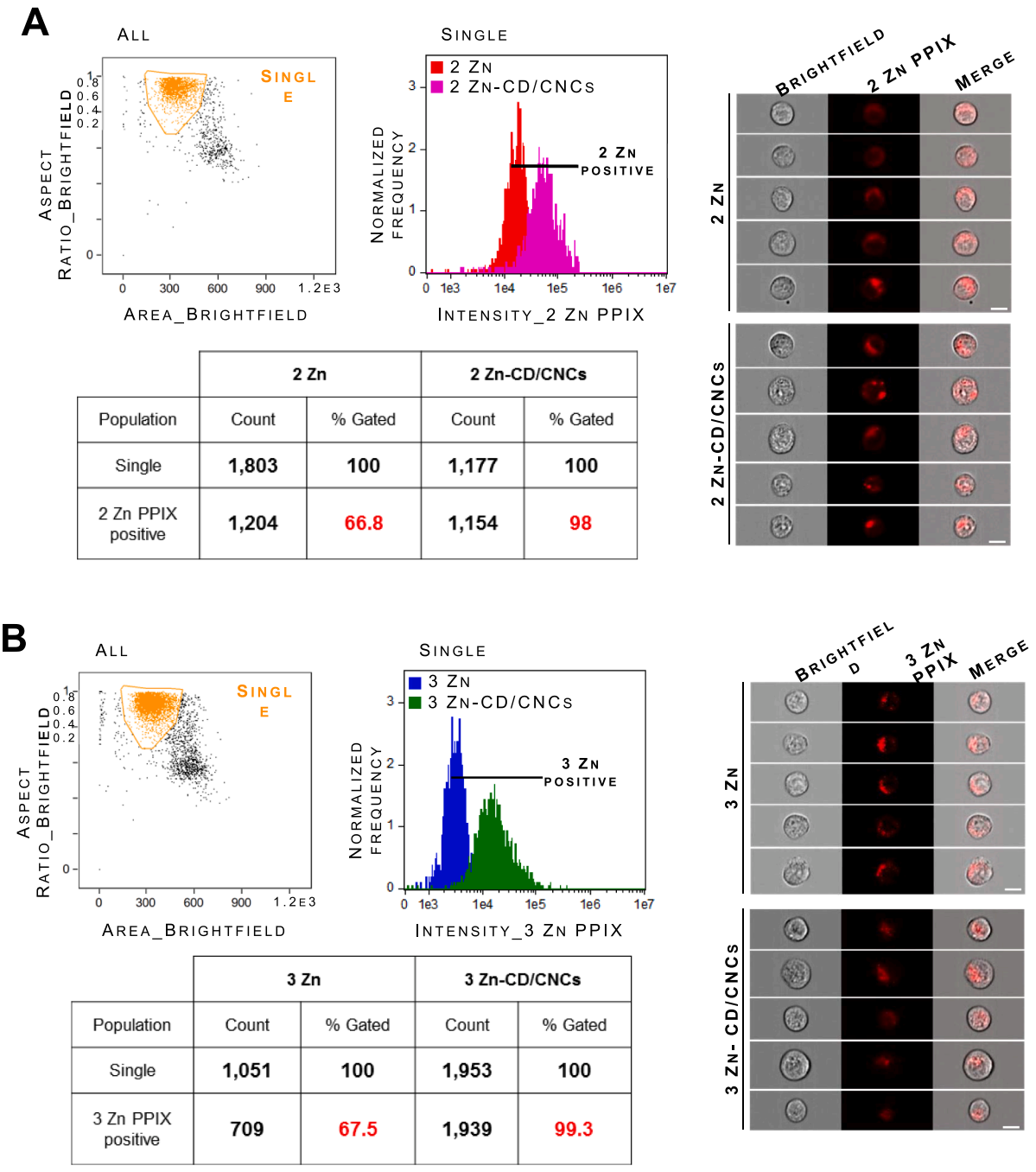

	2 Zn		2 Zn-CD/CNCs	
Population	Count	% Gated	Count	% Gated
Single	1,803	100	1,177	100
2 Zn PPIX positive	1,204	66.8	1,154	98

	3 Zn		3 Zn-CD/CNCs	
Population	Count	% Gated	Count	% Gated
Single	1,051	100	1,953	100
3 Zn PPIX positive	709	67.5	1,939	99.3

Fig. 2. Cell uptake of **2Zn** and **2Zn–CD/CNCs** or **3Zn** and **3Zn–CD/CNCs** by HT-29 cells. HT-29 cells were treated with **2Zn** and **2Zn–CD/CNCs** (A) or **3Zn** and **3Zn–CD/CNCs** (B) at 2.5 μM PPIX. **2Zn** and **3Zn** were solubilized in DMSO and **2Zn-CD/CNCs** and **3Zn-CD/CNCs** in sterilized water. Cell uptake of these compounds was studied through **2Zn** and **3Zn** fluorescence (Exc. 561 nm; Em. 660–740 nm) 24 h post-treatment, by AMNIS® imaging flow cytometry analysis and studied with IDEAS software. The first graph highlights the size/structure of HT-29 cells. Fluorescence intensity of individual HT-29 cells is shown in the second graph and in the representative images (White scale bar = 10 μm). The tables summarize the cell counts and percentages of **2Zn** and **3Zn** positive cells according to the different treatment condition.

intracellular PS fluorescence, although the fluorescence-positive cells only represent 2/3 of the population when incubated with free **2Zn** or **3Zn** at the same concentration (Fig. 2B). This improvement is encouraging for a further use of this nanoplatform in "*in vivo*" experiments.

In conclusion, we describe in this work and for the first time, a new, easy and efficient method for the synthesis of protoporphyrin IX derivatives bearing one and two adamantane groups. The adamantane group has been chosen for this work because it has a strong affinity for the hydrophobic cavity of cyclodextrins and also because it increases the hydrophobic behavior of protoporphyrin IX. Protoporphyrin IX derivatives **2Zn** and **3Zn** were successfully encapsulated into β-cyclodextrin-capped cellulose nanocrystals and all characterizations confirmed the structure of each synthesized compound. All of the compounds presented a low cytotoxicity against HT-29 cells in the dark. In addition, the results obtained by flow cytometry analysis showed a qualitative internalization of the Zn PPIX derivatives with a strong improvement in presence of drug-CD/CNCs. An efficient activity against the HT-29 cancer line was observed with drug-**CD/CNCs** complexes under illumination. Compared to hydrophobic molecules, these complexes have the advantage of forming stable colloidal suspensions in

aqueous media and so they could be easily applied *in vivo*. These results are in agreement with the work of Nakamura et al. who shown similar IC_{50} with PPIX-lipids derivatives (liposomes nanocarriers) againts HeLA cells.[29] In our futur works, studies must then be conducted to highlight the role of these nanocarriers in the targeting of tumor cells thanks to the enhanced permeation and retention effect (EPR). The use of these complexes (β-CD/CNCs) may therefore be a relevant strategy in cancer therapies but also in other pathologies.[30]

Declaration of Competing Interest

The authors declare that they have no known competing financial interests or personal relationships that could have appeared to influence the work reported in this paper.

Acknowledgements

We thank the 'Conseil Régional de Nouvelle Aquitaine' for its financial support. The authors are indebted to Dr. Michel Guilloton for his help in manuscript editing, Pierre Carles (CARMALIM-IRCER – Limoges) for MET analysis and Yves Champavier from BISCEm core facility for NMR analysis.

Appendix A. Supplementary data

Supplementary data to this article can be found online at https://doi.org/10.1016/j.bmcl.2021.128024.

References

1 Alhumaid A, Al Yousef Z, Bakhsh HA, Al Ghamdi S, Azhar Aziz M. *Crit Rev Oncol Hematol*. 2018;132:39–50.
2 Arnold M, Sierra MS, Laversanne M, Soerjomataram I, Jemal A, Bray F. *Gut*. 2017;66:683–691.
3 Karges J, Kuang S, Maschietto F, et al. *Nature Commun*. 2020;11:3262.
4 Dichiara M, Prezzavento O, Marrazzo A, et al. *Eur J Med Chem*. 2017;142:459–485.
5 McFarland SA, Mandel A, Dumoulin-White R, Gasser G. *Curr Opin Chem Biol*. 2020;53:23–27.
6 Sol V, Lamarche F, Enache M, et al. *Bioorg Med Chem*. 2006;14:1364–1377.
7 Taba F, Onoda A, Hasegawa U, et al. *ChemMedChem*. 2018;13:15–19.
8 Sengani M, Grumeszescu AM, Devi Rajeswari V. *OpenNano*. 2017;2:37–46.
9 Reddy LH, Arias JL, Nicolas J, Couvreur P. *Chem Rev*. 2012;112:5818–5878.
10 Dong J, Ghiladi RA, Wang Q, Cai Y, Wei Q. *Nanotechnology*. 2018;29, 265601.
11 Shibano M, Nishida S, Saito Y, Kamitakahara H, Takano T. *Carbohydr Polym*. 2014;113:279–285.
12 Ndong Ntoutoume GMA, Grassot V, Chabanais J, Petit JM, Granet R, Sol V. *Carbohydr Polym*. 2017;164:258–268.
13 Domingues RMA, Silva M, Gershovich P, et al. *Bioconjug Chem*. 2015;26:1571–1581.
14 Drogat N, Granet R, Le Morvan C, Bégaud-Grimaud G, Krausz P, Sol V. *Bioorg Med Chem Lett*. 2012;22:3648–3652.
15 Wang N, Ding E, Cheng R. *Polymer*. 2007;48:3486–3496.
16 Habibi Y, Hoeger I, Kelly SS, Rojas OJ. *Langmuir*. 2010;26:990–1001.
17 Liu Tianjun, Yang Shu 刘天军, 杨 2013 CN 104130266 A 20141105.
18 Montalbetti CAGN, Falque V. *Tetrahedron*. 2005;61:10827–10852.
19 Ormond BA, Freeman SH. *Dyes Pigm*. 2013;96:440–448.
20 Jiblaoui A, J. Brevier J, Ducourthial G, Gonzales-Nunez H, Baudequin C, Sol V, Lhez-Leroy S, Tetrahedron, 2015, 71, 2428-2434.
21 Ndong Ntoutoume GMA, Granet R, Mbakidi JP, et al. *Bioorg Med Chem Lett*. 2016;26:941–945.
22 Spinella S, Maiorana A, Qian Q, et al. *ACS Sustainable Chem Eng*. 2016;4:1538–1550.
23 Moon RJ, Martini A, Nairn J, Simonsen J, Youngblood J. *Chem Soc Rev*. 2011;40:3941–3994.
24 Grishkewich N, Mohammed N, Tang J, Tam CK. *Curr Opin Colloid Interface Sci*. 2017;29:32–45.
25 Hasani M, Cranston ED, Westman G, Gray DG. *Soft Matter*. 2008;4:2238–2244.
26 Jordan HJ, Easson MW, Condon BD. *Nanomaterials*. 2019;9:1232.
27 Zhang H, Qian Y, Chen S, Zhao Y. *Food Hydrocolloids*. 2019;96:267–277.
28 Lin N, Dufresne A. *Biomacromolecules*. 2013;14(3):871–880.
29 Tachikawa S, El-Zaria ME, Inomata R, Sato S, Nakamura H. *Bioorg Med Chem*. 2014;22:4745–4751.
30 Caillaud M, Msheik Z, Ndong Ntoutoume GMA, et al. *Free Radical Biol Med*. 2020;161:246–262.